Fusion rates from resonant states of $td\mu$

P. Froelich and A. Flores-Riveros
Department of Quantum Chemistry, Uppsala University, Box 518, S-751 20 Uppsala, Sweden

S. A. Alexander
Institute for Astrophysics and Planetary Exploration, Department of Physics, University of Florida, Gainesville, Florida 32611
(Received 12 December 1991)

The structure of the continuous spectrum of the muonic molecular ion $td\mu$ has been investigated. We have calculated the energies, lifetimes, geometries, and fusion rates of several resonances having angular momentum $J=0$ in the neighborhood of the $(t\mu)_{2S}$ threshold. The significance of these states for muon-catalyzed fusion under high-temperature conditions is discussed.

PACS number(s): 31.20.Di, 36.10.Dr

I. INTRODUCTION

In the reaction chain leading to muon-catalyzed fusion [1], the formation of $td\mu$ occurs most efficiently at a resonant collision energy corresponding to ~ 1600 K [2,3]. This resonant mechanism, proposed by Vesman [4], involves the transfer of collisional and binding energy into the rovibrational degrees of freedom of the host molecule D_2 in the reaction

$$t\mu+(D_2)_{v_i,K_i}\rightarrow\langle(td\mu)^{J,v}dee\rangle_{v_f,K_f} . \quad (1)$$

It is the amount of energy that can be transferred to the rovibrational degrees of freedom of the host molecule which dictates the optimal temperature. Vesman's resonant mechanism is dependent on the existence of intact D_2 host molecules and can occur only at collisional energies smaller than their dissociation energy of ~ 4.5 eV.

Recently, there has been an increased interest in muon-catalyzed fusion at temperatures corresponding to a "tepid" plasma (5–50 eV) [5–9]. At these temperatures, Vesman's mechanism no longer operates because the deuterium-tritium fuel is dissociated and at least partially ionized. In partially ionized plasmas, however, the mesomolecules can be formed at high rates (comparable with Vesman's mechanism) via three-body collisions [8,10] and via direct, resonant collisions [6,7]. It is this last process that we address in the present work, but it should be emphasized that both mechanisms can coexist and contribute to the final fusion yield at high temperatures.

Originally, the concept of having muon-catalyzed fusion take place in plasma was proposed in order to increase the muon reactivation rate. Menshikov suggested [9] that muon stripping in a plasma with $\phi=1$ liquid-hydrogen density (LHD) and $T=100$ eV would be $\sim 60\%$, a factor of 2 improvement compared to the molecular reactivation. Since then, it has become clear that calculations of reactivation in plasmas are very sensitive to how the plasma stopping power is modeled. Using a plasma stopping power based on the random-phase approximation, Jändel, Froelich, and Larson found that reactivation was considerably enhanced first at energies above a few hundred electron volts [11]. At these temperatures the mesomolecular formation rate via three-body collisions is very low [10] and for a fully ionized plasma even muon capture becomes difficult [12]. In order to ensure both high-resonant or quasiresonant (three-body) molecular-formation rates *and* high reactivation rates, Menshikov [9] has proposed the concept of an inhomogeneous plasma where formation would occur in a dense molecular phase and the reactivation would occur in a plasma.

In order for muon-catalyzed fusion to occur rapidly, a window of physical conditions is needed where *both* the rate of muonic molecule formation is high *and* the effective sticking is low. Below we will show that the existence of resonances may lead to direct molecular formation, a process that is possible at high temperatures and without a molecular environment. The resonant lifetimes and formation rates are sufficiently high to allow direct fusion from resonant states. Such a combination might permit efficient muon-catalyzed fusion in homogeneous plasmas.

In the three-body collision, the mesomolecule is formed via the reaction

$$t\mu+d+X\rightarrow(td\mu)+X' . \quad (2)$$

The third body (X) can be an electron, a nucleon, a neutral atom, or a molecule, although the highest formation rates are obtained for electrons [10]. In a resonant collision, the mesomolecule can be formed directly (without a third body) in the metastable state [7].

$$t\mu+d\rightarrow(td\mu)^* . \quad (3)$$

Because the metastable state can fuse, the above reaction can be looked upon as an example of resonantly enhanced fusion in flight. The metastable state can also back decay or be deexcited to a lower bound state and fuse from there. In particular, the deexcitation process may occur via collisions with free plasma electrons whereby the electron carries away excess excitation energy. Such collisions provide a very effective means of deexcitation in dense ($\phi=0.1-1.0$ LHD) plasmas [13].

Fast resonant formation rates are not confined to plasma conditions. The high-energy particles which collide during the thermalization of $d\mu$ and $t\mu$ atoms are repeatedly reaccelerated during the deexcitation cascade [14] [e.g., a $(t\mu)_n$ atom formed via muon exchange from a $(d\mu)_n$ atom acquires an initial kinetic energy of about $19/n^2$ eV]. The high rate of epithermal formation in the direct resonance reactions may introduce additional paths in the prevailing kinematic picture of the muon catalyzed fusion (μCF) chain and lead to perturbations in the muon cycling rate.

II. CALCULATION OF RESONANT STATES

Recent calculations demonstrated the existence of three-body resonances in $td\mu$ [5–7,15]. Despite their relatively high energy [54 eV above the $(t\mu)_{1S}$ threshold and 6 eV above the $(d\mu)_{1S}$ threshold for the lowest resonance], the formation rate of some of these states has been estimated to be of the same order of magnitude as the typical formation rates given by Vesman's mechanism [16]. This discovery encouraged us to search for other $td\mu$ resonances in the hope of finding some with still lower binding energy. Such states are especially interesting because their formation rate increases with decreasing collisional energy and because it is easier to confine a plasma at the corresponding (low) resonant energy.

The resonances in Refs. [5–7] were obtained from a variational calculation using a basis of generalized Hylleraas functions. The bulk of the numerical effort was connected to the solution of the real matrix eigenvalue problem. The lifetimes of these states were calculated by means of the stabilization method, a simplified version of the complex-coordinate method (CCM), which uses analytical continuation of the stabilization graphs.

The present calculations are also variational but use basis sets of random tempered Slater geminals [17–20]. This wave-function form seems to give very accurate values for diffuse states and produced a very accurate binding energy for the $td\mu(1,1)$ state (660.1526 meV) [20]. The main improvement over the calculations in Refs. [5–7] is that now we have implemented the exact CCM. This method requires the solution of the complex matrix eigenvalue problem. The details of the CCM can be found elsewhere [21], here we will only recall that one studies the spectral properties of the dilated Hamiltonian

$$H(\Theta)=U(\Theta)HU^{-1}(\Theta)\ , \tag{4}$$

where the transformation $U(\Theta)$ is defined as

$$Uf(\mathbf{r})=e^{3\Theta/2}f(e^{\Theta}\mathbf{r}) \tag{5}$$

and where Θ is a complex dilation parameter $\Theta=s+i\eta$. The explicit form of the dilated Hamiltonian for the $td\mu$ molecular ion is

$$H(\Theta)=-\frac{e^{-2\Theta}}{2}\nabla_{t\mu}^2-\frac{e^{-2\Theta}}{2}\left[\frac{m_{t\mu}}{m_{d\mu}}\right]\nabla_{d\mu}^2 -e^{-2\Theta}\left[\frac{m_{t\mu}}{M_{\mu}}\right]\nabla_{t\mu}\cdot\nabla_{d\mu}-\frac{e^{-\Theta}}{r_{t\mu}}-\frac{e^{-\Theta}}{r_{d\mu}}+\frac{e^{-\Theta}}{r_{td}}\ , \tag{6}$$

where $\mathbf{r}_{t,\mu}$ and $\mathbf{r}_{d\mu}$ are the vectors from the muon to the triton and deuteron, respectively; r_{td} denotes the distance between the nucleons; $m_x=M_{\mu}M_x/(M_{\mu}+M_x)$ is the reduced mass of the $t\mu$ or $d\mu$ system and the values of M_t, M_d, and M_{μ} are 5496.899, 3670.481, and 206.7686, respectively (in units of electron mass). In a stabilization calculation the scaling parameter Θ assumes only real values. In the exact implementation of the CCM the continuous spectrum of the dilated Hamiltonian is rotated out in the complex plane by the angle 2η around the consecutive thresholds. For the $td\mu$ system, such a rotation separates the branches belonging to the $t\mu+d$ and $d\mu+t$ thresholds. The bound states remain uninfluenced by this transformation, whereas the discrete complex spectrum of the dilated eigenvalue problem

$$H(\Theta)\Psi=E\Psi \tag{7}$$

corresponds to the resonances.

In our calculations, the wave functions for each $td\mu$ resonance having angular momentum $J=0$ are computed using the form [17–20]

$$\Psi=\sum_{i=1}^{N}c_i e^{-\alpha_i r_{t\mu}-\beta_i r_{d\mu}-\gamma_i r_{td}}\ . \tag{8}$$

The nonlinear parameters in these Slater geminals have been generated using the tempering formulas [17]

$$\begin{aligned}\alpha_i&=|A_1\langle i,1\rangle+A_2\langle i,4\rangle|\ ,\\ \beta_i&=|B_1\langle i,2\rangle+B_2\langle i,5\rangle|\ ,\\ \gamma_i&=|C_1\langle i,3\rangle+C_2\langle i,6\rangle|-\min(\alpha_i,\beta_i)\ ,\end{aligned} \tag{9}$$

where A_1, A_2, B_1, B_2, C_1, and C_2 are the tempering parameters, $\langle k,j\rangle$ is the fractional part of $\{[k(k+1)/2][P(j)]^{1/2}\}$ and $P(j)$ is the jth prime number in the sequence 2,3,5,7,.... For the $td\mu$ ground state, the tempering parameters were calculated so as to minimize the ground-state energy with a set of 100 basis functions. The resulting values are listed in the first column of Table I. Because the variational principle cannot be applied to resonance states, we were unable to optimize tempering parameters for these states. Instead, we chose a set which gave a good representation of all resonances of interest on a real stabilization plot. These parameters are also listed in Table I. Since the tempering parameters for the resonance states are not the optimal ones, the convergence of these calculations are expected to be slower than that of any of the bound states.

TABLE I. Tempering parameters for $td\mu$ states using the Slater geminal basis.

	Ground state	Resonant states
A_1	1.271 120 65	1.271 120 65
B_1	1.368 897 28	1.368 897 28
C_1	3.093 182 89	1.237 273 00
A_2	−0.135 864 89	−0.135 864 89
B_2	−0.230 165 24	−0.230 165 24
C_2	−0.016 219 88	−0.006 488 00

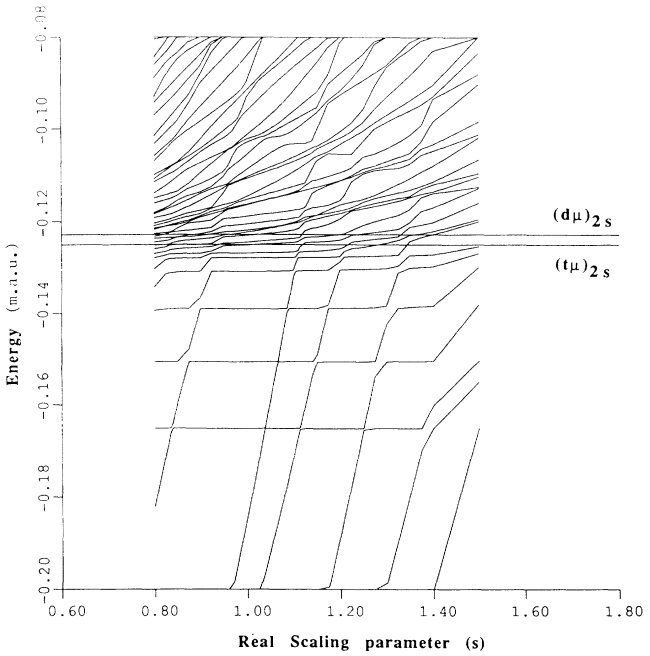

FIG. 1. General view (in muon atomic units) of the discretized continuous spectrum of $td\mu$ near the $(t\mu)_{2S}$ threshold as a function of the real scaling parameter ($\Theta=s$). $K=600$. Also shown are the $(t\mu)_{2S}$ and $(d\mu)_{2S}$ thresholds.

The coefficients c_i in Eq. (8) are obtained by solving the complex non-Hermitian matrix eigenvalue problem

$$\underline{H}\,\underline{c}_i = E_i \underline{c}_i \tag{10}$$

for those states that are stable with respect to variations in the dilation parameter Θ. The energies and widths of

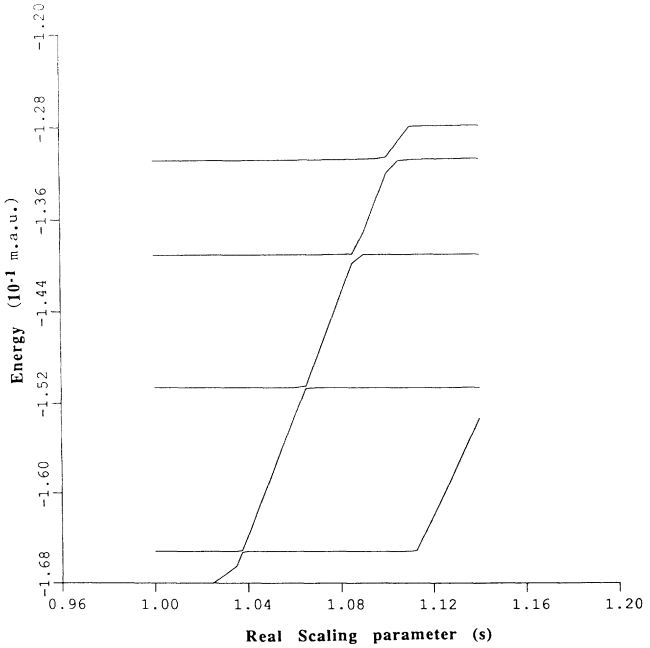

FIG. 2. Expanded view (in muon atomic units) of the lowest four avoided crossings of $td\mu$ near the $(t\mu)_{2S}$ threshold as a function of the real scaling parameter ($\Theta=s$). $K=600$.

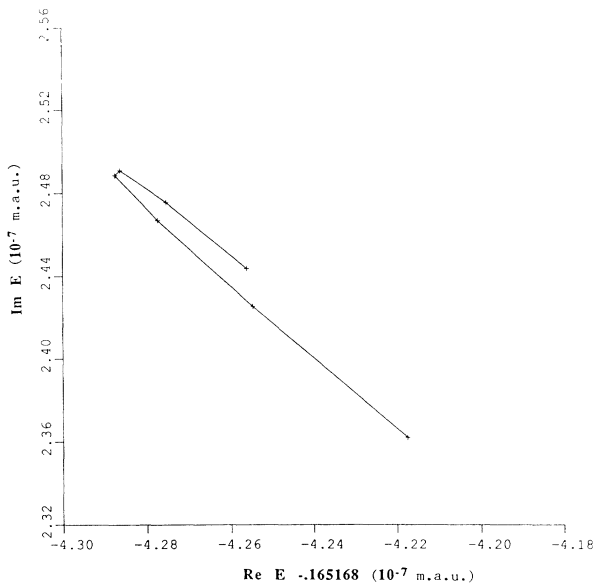

FIG. 3. Trajectory (in muon atomic units) of the resonant root at $-0.165\,168$ m.a.u. as a function of the dilation angle. $K=600$, $s_{\min}=0.9683$, $\Delta\eta=0.0125$.

the resonant states are obtained from the real and imaginary parts of these complex eigenvalues ($E_r - i\Gamma/2$). To determine exactly which roots are stable with respect to variations in the dilation parameter, we first performed a real scaling calculation. This step provides a general view of the structure of the continuous spectrum as a function of the scaling parameter ($\Theta=s$) and gives the approximate position of the detected resonances. Such a graph, signalling the presence of several resonances, is presented in Figs. 1 and 2. Next, we made a detailed

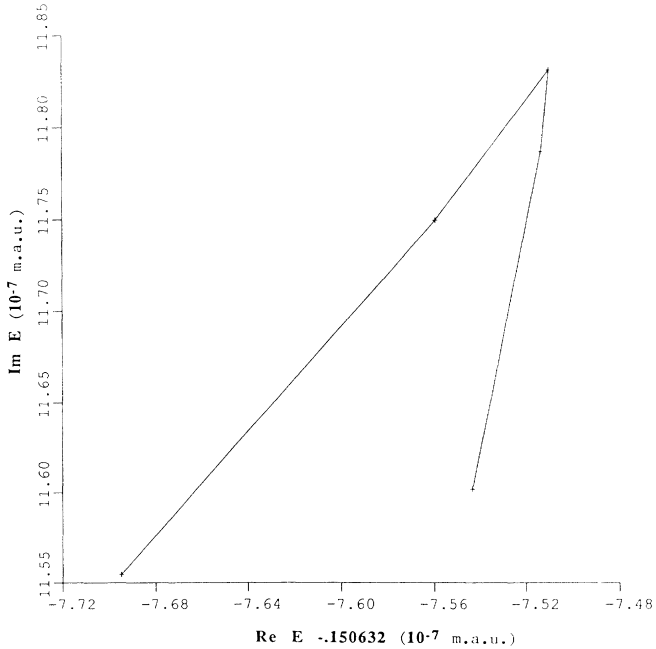

FIG. 4. Trajectory (in muon atomic units) of the resonant root at $-0.150\,633$ m.a.u. as a function of the dilation angle. $K=600$, $s_{\min}=0.9683$, and $\Delta\eta=0.01$.

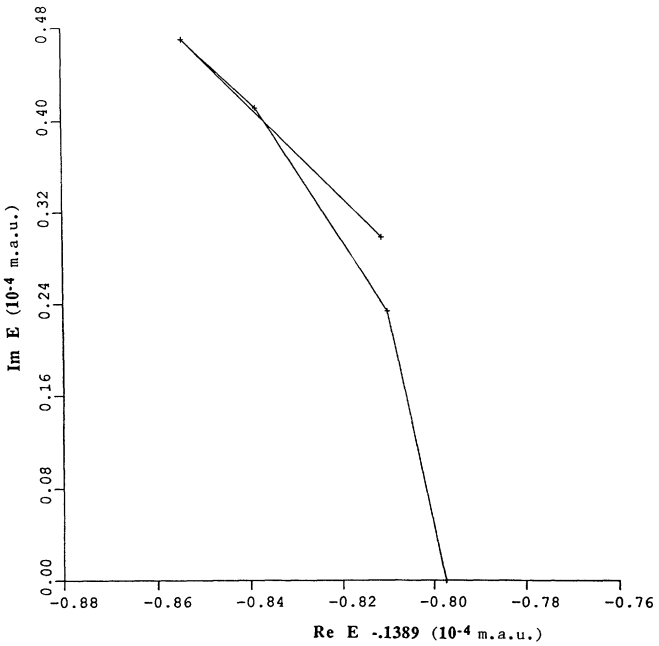

FIG. 5. Trajectory (in muon atomic units) of the resonant root at $-0.138\,985$ m.a.u. as a function of the dilation angle. $K=600$, $s_{\min}=0.9683$, $\Delta\eta=0.025$.

study of each individual resonance by stabilizing each eigenvalue approximating that resonance with respect to variations in the complex dilation parameter Θ such that

$$\frac{\partial E}{\partial \Theta}=0 . \tag{11}$$

To find these stable values, we have used the complex virial theorem [22–24], i.e., we have minimized the virial

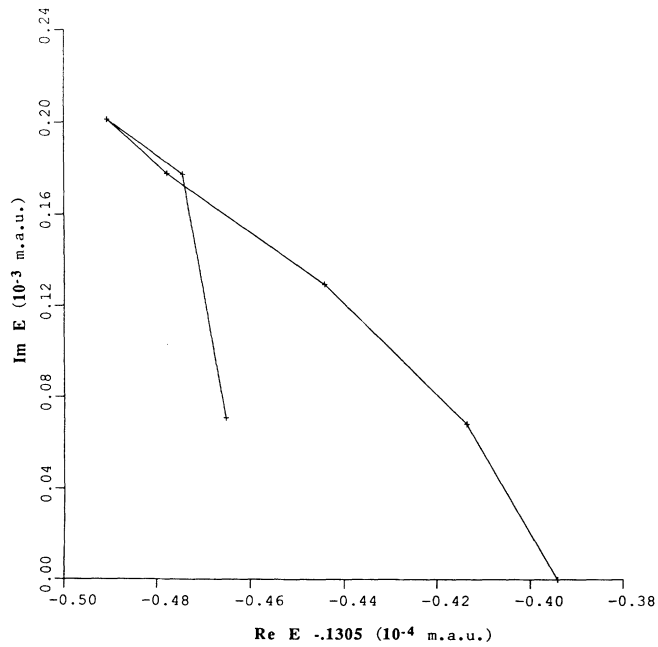

FIG. 6. Trajectory (in muon atomic units) of the resonant root at $-0.130\,549$ m.a.u. as a function of the dilation angle. $K=600$, $s_{\min}=0.9683$, and $\Delta\eta=0.05$.

with respect to the complex dilation parameter Θ such that

$$|2\langle T(\Theta)\rangle+\langle V(\Theta)\rangle|=\text{minimum} , \tag{12}$$

where $\langle T(\Theta)\rangle$ is the expectation value of the kinetic energy with respect to the appropriate eigenfunction and $\langle V(\Theta)\rangle$ is the expectation value of the potential energy. For this method to work, Eq. (12) must be optimized to a value that is smaller than the width of the resonance. The stationary behavior of those complex eigenvalues that represent resonances is illustrated in Figs. 3–6. In these complex rotation calculations, we show the behavior of the real and imaginary components of the energy as a function of $\Theta=s_{\min}+j\Delta\eta$, where $j=0,1,2,\ldots$. The presence of a cusp or turning point at $\Theta=s_{\min}+\eta_{\min}$ signals the presence of a resonance.

III. RESULTS AND DISCUSSION

The results of our calculations on each resonance state using the CCM are presented in Table II. These resonances seem to cluster just below the $(t\mu)_{2S}$ threshold, and their exact number is unknown. In general, the magnitude of both the widths and the average internuclear distances increase as the resonances approach the threshold. For comparison, we also include the corresponding information about the $J=0$ bound states [17–19].

The fusion rates from the resonant states are reported in the last column of Table II. Surprisingly, these rates do not decrease with the increased size of the metastable molecules. Such behavior was already suggested by the fusion rates from the bound excited molecular states and in Ref. [19] was related to the fact that an increase in the excitation energy causes an inward shift of the classical turning point. It is interesting to note that some of the resonances in Table II live long enough to allow for fusion during a single lifetime.

In addition to the resonances listed in Table II, we observed the existence of several resonant states just below the $(t\mu)_{2S}$ threshold. An expanded view of this region is shown in Fig. 7. Although we were not able to accurately describe these states using the CCM because of the size of the basis-set expansion needed, we were able to estimate their energy by using large real scaling calculations. The results, summarized in Table III, suggest that these values have converged to at least three significant figures except for the two highest "resonances." It should be emphasized, however, that these simple real-scaling calculations cannot precisely determine resonance positions. When the full CCM is used, these energies can shift slightly.

In Table IV we present the results of earlier $td\mu$ resonance calculations. The positions and geometries of the resonances in Ref. [15] are generally in good agreement with ours, but the widths differ considerably in some cases. While the convergence of the energies, geometries, and fusion rates of our resonance states is slower than for the bound states (see Table II), it is still sufficient to produce a satisfactory accuracy. In contrast, however, the lifetime of our resonances seem to converge slowly. With our current algorithms, larger basis-set sizes are compu-

TABLE II. Properties of $td\mu$ states with angular momentum $J=0$. The lifetime is given in seconds, the geometries in absolute muon atomic units, and the fusion rate in seconds^{-1}.

E (m.a.u.)[a]	E (eV)[b]	Width (eV)	Lifetime	Basis[c]	$\langle r_{t\mu}\rangle$	$\langle r_{d\mu}\rangle$	$\langle r_{td}\rangle$	λ_f
−0.558 854		$td\mu(0,0)$ bound state[d]		S 600	1.95	2.04	2.65	0.69[12]
−0.558 854		$td\mu(0,0)$ bound state[d]		S 1400	1.95	2.04	2.65	0.69[12]
−0.506 424		$td\mu(0,1)$ bound state[d]		S 600	2.64	3.79	4.97	0.60[12]
−0.506 424		$td\mu(0,1)$ bound state[d]		S 1400	2.64	3.79	4.97	0.58[12]
−0.5		$(t\mu)_{1S}$ threshold		exact	1.5	infinity	infinity	$\sim 10^{6}$[e]
−0.491 140		$(d\mu)_{1S}$ threshold		exact	infinity	1.527	infinity	$\sim 10^{6}$[e]
−0.165 168	−217.812	0.0027	2.44[−13]	S 600	6.06	6.21	9.83	4.92[12]
−0.150 633	−138.996	0.0128	5.14[−14]	S 600	7.03	7.31	11.87	2.21[13]
−0.138 985	−75.834	0.5124	1.28[−15]	S 600	8.24	9.11	14.85	1.22[13]
−0.130 549	−30.090	2.1848	3.01[−16]	S 600	8.69	14.78	20.92	2.75[14]
−0.125	0.0	$(t\mu)_{2S}$ threshold		exact	6.0	infinity	infinity	$\sim 10^{6}$[e]
−0.122 785	12.011	$(d\mu)_{2S}$ threshold		exact	infinity	6.108	infinity	$\sim 10^{6}$[e]

[a]Binding energy is given in muon atomic units defined as $-2\,E_{1s}^{t\mu}=1$ m.a.u.$=5422.5347$ eV.
[b]Excitation energy is given in eV relative to the $(t\mu)_{2S}$ threshold at -0.125 m.a.u.
[c]S=Slater wave function.
[d]Values from Refs. [17–19].
[e]Typical rate for fusion in flight.

tationally too expensive to perform since we must solve for all complex eigenvalues. To avoid this problem we have experimented with the complex version of the inverse iteration method but found that this procedure has difficulty resolving near-degenerate eigenvalues such as those produced by a complex rotation. Clearly more work is needed in this area to more accurately resolve the lifetimes of these states.

With the exception of the very highest resonance, all of the $K=1800$ binding energies listed in Table III are lower (and presumably more accurate) than those computed by Hara and Ishihara [25]. Although the behavior of the eigenvalues just below the $(t\mu)_{2S}$ threshold is rather complicated, we see no evidence of a resonance near -1.600 eV.

Although not included in Tables II or III, we also saw some evidence in our Slater geminal calculations of the lower resonance described in Refs. [5–7]. Unfortunately we were unable to obtain a satisfactory result for this state by performing a CCM calculation with a $K=600$ basis. It seems likely that this resonance is not accurately described by the same set of parameters (given in Table I) that we used to compute the resonances just below the $(t\mu)_{2S}$ threshold.

Because several resonant states cluster just below the $(t\mu)_{2S}$ threshold, they may play a significant role in the mesocatalytic fusion chain. It is important to realize that the collisional energy which leads to the formation of these highly excited states does not have to be high, since it should be measured with respect to the closest threshold (and not with respect to the lowest threshold). For instance, with respect to the $2S$ threshold is less than the dissociation energy of D_2 then it can be formed via

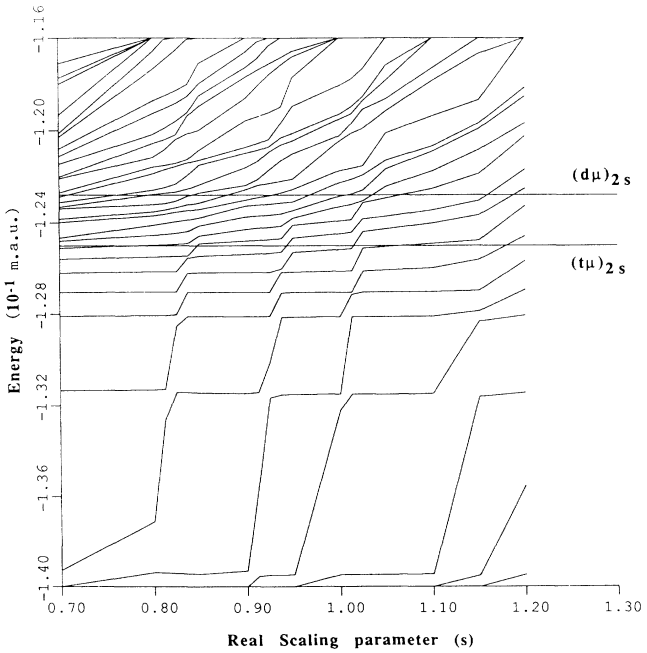

FIG. 7. Expanded view (in muon atomic units) of the discretized continuous spectrum of $td\mu$ near the $(t\mu)_{2S}$ threshold as a function of the real scaling parameter ($\Theta=s$). $K=900$. Also shown are the $(t\mu)_{2S}$ and $(d\mu)_{2S}$ thresholds.

TABLE III. Binding energies (in eV) of resonances below the $(t\mu)_{2S}$ threshold. K is the number of basis functions used.

$K=900$	$K=1200$	$K=1500$	$K=1800$
−217.883	−217.889	−217.891	−217.892
−139.833	−139.715	−139.728	−139.731
−78.690	−79.049	−79.103	−79.118
−35.781	−36.455	−36.573	−36.610
−17.126	−17.394	−17.443	−17.460
−11.219	−11.388	−11.413	−11.422
−6.605	−7.087	−7.214	−7.245
−2.036	−2.978	−3.408	−3.555[a]

[a]This energy is within the range of the Vesman formation mechanism.

TABLE IV. Literature values of resonances with angular momentum $J=0$. The geometries are given in absolute muon atomic units.

E (eV)[a]	Width (eV)	Basis[b]	$\langle r_{t\mu}\rangle$	$\langle r_{d\mu}\rangle$	$\langle r_{td}\rangle$	Reference
−1979.106	0.74	H 1158	7.49	7.99	13.92	7
−217.889	0.036	H 1101	6.29	6.44	10.19	17
−217.892		M 2200				27
−139.521	0.076	H				17
−139.724		M 2200				27
−78.404	1.125	H				17
−79.095		M 2200				27
−36.567		M 2200				27
−17.443		M 2200				27
−11.414		M 2200				27
−7.225		M 2200				27
−3.565		M 2200				27
−1.600		M 2200				27

[a]All binding energies adjusted to be relative to the $(t\mu)_{2S}$ threshold at −0.125 m.a.u.
[b]H = Hylleraas wave function, M = molecular wave function in spheroidal coordinates.

Vesman's mechanism [4]. Indeed, Table III presents one such resonance.

Resonances with energies more than 4.5 eV below the $2S$ threshold can be formed by the direct (Auger) mechanism or in three-body collisions (which have been shown to play an important role in the formation of bound states [8,10]). In such situations excess collisional and binding energy is carried away by a third-body partner. These formation processes can take place in the presence of excited $(t\mu)_{2S}$ or $(d\mu)_{2S}$ atoms during the cascade associated with the thermalization of captured muons. Due to the dipole-moment character of Vesman's formation mechanism and because of their large size (see Table II), resonant states can be formed much faster than the bound states below the $(t\mu)_{1S}$ threshold. For some of the resonant states in Table II, the formation rate can reach values as high as 10^{11} sec^{-1}, some two orders of magnitude faster than the Vesman mechanism for bound states.

The formation of resonances may also influence the muon-exchange process. Since muon exchange from excited $d\mu$ states is very fast compared to electromagnetic or collisional deexcitation, most muons that reach the thermalized $t\mu$ state will undergo the exchange process from excited $2S$ states. Such reactions are likely to proceed via resonant states. The problem is further complicated by the fact that muon-exchange reactions via resonant states compete with fusion, i.e., each time a resonant state is formed it can either decay or fuse. Some of the resonances in Table II have a lifetime comparable to the time required for fusion, and once formed, will certainly fuse. Even those resonances that have a lifetime shorter than their fusion time may play important roles if repeated formations can occur. This situation is possible if the system is thermalized at the resonant energy but is inhibited by the thermalization process (see, for example, Ref. [11]).

The influence of resonant states on the μCF cycle is determined by the competition between the muonic atom deexcitation, nonresonant muon exchange, and the formation rate of resonant states at each energy during the thermalization process. We should point out, however, that the collisional cross section for the muon exchange peaks at the resonant energies and that the nonresonant process has considerable probability only at velocities compatible with those of internal motion of the muon. Without knowing the detailed kinetics of the thermalization process in the presence of the various resonant states, it is difficult to predict precisely what fraction of the muon transfer is due to the intermediate resonance formation. What is clear is that the branching ratio of the resonant decay into different channels ($t\mu$, $d\mu$, fusion, or deexcitation) is an important quantity that regulates the impact of each resonance on the kinetics of μCF.

If a significant fraction of fusion from resonant states were to occur in conventional (low-temperature) μCF experiments, one would expect that the apparent (i.e., experimentally observed) fusion rate would depend on the mixture density. This dependence is probably different for resonances just above the $(t\mu)_{1S}$ threshold (such as those reported in Ref. [5]) and just below $(t\mu)_{2S}$ threshold. At higher density, the rate of formation of the below-threshold resonances tends to increase because it is likely to follow a Vesman or three-body-type mechanism. On the other hand, high density leads to fast thermalization which inhibits the direct resonant formation of the above threshold resonances. Since the direct resonant mechanism is fastest, the above threshold resonances might be more important and their overall influence would grow with decreased density. Thus it is the external conditions (such as temperature and density) together with the kinetics of deexcitation and thermalization that decide whether the system can be driven towards fusion from resonant states whose fusion rates and sticking fractions are different from those of the bound states.

In conclusion we have shown that the lifetimes of some resonances of $td\mu$ may be comparable with their fusion rates. This may have a number of important implications for the μCF reaction chain. In addition, the proximity of some resonances to the $(t\mu)_{2S}$ threshold could lead to rapid formation rates. These findings suggest that the excited state (and nonequilibrium) chemistry of μCF should be investigated in greater detail.

ACKNOWLEDGMENTS

This work has been supported by the Swedish National Science Research Council. We would also like to thank the staff of the Northeast Regional Data Center for their support in running our program on the University of Florida IBM 3090 and the staff of the Swedish National Supercomputer Center for time on the CRAY XMP in Linköping.

[1] P. Froelich, Europhys. News **20**, 57 (1989).
[2] M. Leon, Phys. Rev. Lett. **52**, 605 (1984).
[3] J. S. Cohen and M. Leon, Phys. Rev. Lett. **55**, 52 (1985).
[4] E. Vesman, Pis'ma Zh. Eksp. Teor. Fiz. **5**, 113 (1967) [JETP Lett. **5**, 91 (1967)].
[5] P. Froelich and K. Szalewicz, Phys. Lett. A **129**, 321 (1988).
[6] P. Froelich and K. Szalewicz, Muon Catal. Fusion **3**, 345 (1988).
[7] P. Froelich, K. Szalewicz, H. J. Monkhorst, W. Kolos, and B. Jeziorski, in *Muon-Catalyzed Fusion*, Proceedings of a conference on Muon-Catalyzed Fusion held on Sanibel Island, Florida, 1988, edited by S.E. Jones, J. Rafelski, and H. J. Monkhorst, AIP Conf. Proc. No. 181 (AIP, New York, 1989).
[8] L. Menshikov and L. Ponomarev, Pis'ma Zh. Eksp. Teor. Fiz. **46**, 246 (1987) [JETP Lett. **46**, 312 (1987)].
[9] L. Menshikov and V. Shakirov, Zh. Eksp. Teor. Fiz. **95**, 458 (1989) [Sov. Phys. JETP **68**, 258 (1989)].
[10] L. Menshikov, I. V. Kurchatov Institute of Atomic Energy Tech. Rep. No. IAE-4589/2, Moscow, 1988 (unpublished).
[11] M. Jändel, P. Froelich, and G. Larson, Phys. Rev. A **40**, 2799 (1989).
[12] P. Froelich, H. J. Monkhorst, and C. Stodden (unpublished).
[13] P. Froelich and A. Adamczak (unpublished).
[14] L. Menshikov, Muon Catal. Fusion **2**, 173 (1988).
[15] C. Y. Hu and A. K. Bhatia, Phys. Rev. A **43**, 1229 (1991).
[16] P. Froelich and K. Szalewicz (unpublished).
[17] S. A. Alexander and H. J. Monkhorst, Phys. Rev. A **38**, 26 (1988).
[18] A. Scrinzi, H. J. Monkhorst, and S. A. Alexander, Phys. Rev. A **38**, 4859 (1988); **39**, 3705(E) (1989).
[19] S. A. Alexander, P. Froelich, and H. J. Monkhorst, Phys. Rev. A **41**, 2854 (1990); **43**, 2585(E) (1991).
[20] S. E. Haywood, S. A. Alexander, and H. J. Monkhorst, Phys. Rev. A **43**, 5847 (1991).
[21] W. Reinhardt, Ann. Rev. Phys. Chem. **33**, 223 (1982).
[22] P. Froelich, M. Hehenberger, and E. Brandas, Int. J. Quantum Chem. **11**, 295 (1977).
[23] E. Brandas and P. Froelich, Phys. Rev. **16**, 2207 (1977).
[24] P. Froelich and S. A. Alexander, Phys. Rev. A **42**, 2550 (1990).
[25] S. Hara and T. Ishihara, Phys. Rev. A **40**, 4232 (1989).